# Advances in Ultrafast Control and Probing of Correlated-Electron Materials

Simon Wall, Matteo Rini, Sarnjeet S. Dhesi, Robert W. Schoenlein, and Andrea Cavalleri

***Abstract*—In this paper, we present recent results on ultrafast control and probing of strongly correlated-electron materials. We focus on magnetoresistive manganites, applying excitation and probing wavelengths that cover the mid-IR to the soft X-rays. In analogy with near-equilibrium "filling" and "bandwidth" control of phase transitions, our approach uses both visible and mid-IR pulses to stimulate the dynamics by exciting either charges across electronic bandgaps or specific vibrational resonances. X-rays are used to unambiguously measure the microscopic electronic, orbital, and structural dynamics. Our experiments dissect and separate the nonequilibrium physics of these compounds, revealing the complex interplay and evolution of spin, lattice, charge, and orbital degrees of freedoms in the time domain.**

***Index Terms*—Manganites, photoinduced phase transitions, ultrafast spectroscopy, vibrational excitation.**

## I. Strongly Correlated Materials

STRONGLY correlated-electron materials exhibit many remarkable properties, ranging from high temperature superconductivity to colossal magnetoresistance (CMR), which may lead to important technological applications. Their interesting features are the result of the complex coupling between spin, charge, lattice, and orbital degrees of freedom, which concur in determining the stable phases of these solids. Manipulation of one of these microscopic parameters, for example, by chemical doping, which controls the available charge in unfilled bands, generates an abundance of new phases, often with drastically different properties. These multiple phases often possess similar free energies, enabling relatively weak external stimuli to drive a material across phase boundaries.

At the heart of correlated-electron physics is the concept of a Mott insulator [1]. In this model, which captures several properties of complex materials, electrons hop to unoccupied states and thereby lower their energy by $t$, the hopping or transfer energy. This competes with the repulsive Coulomb interaction, which raises their energy by an amount $U$, the electrostatic onsite repulsion between two electrons. The ability of the material to conduct is then dependent upon the relative strength of the hopping, which delocalizes electrons, with respect to the Coulomb term, which localizes them.

The picture presented by Mott also provides an intuitive explanation for the sensitivity of correlated materials to perturbation. By changing the charge distribution, or filling, e.g., by doping, the electronic density is changed, thus enhancing or diminishing the role of Coulomb interactions. Likewise, modifying the electron hopping, e.g., by changing bond angles, can also promote or hinder charge delocalization. Statically, transitions that result from changing the charge density are called "filling-controlled" phase transitions, while those that result from changes to the electron hopping are called "bandwidth-controlled" phase transitions.

The characteristics of Mott insulators are conceptually different from those of conventional band materials, in which the band structure is generated by the symmetry of the lattice alone. In these materials, the band structure remains rigid and independent on the number and distribution of charges within the material.

This difference is apparent in the ultrafast response of correlated materials, which can be associated with colossal changes in their properties [2], often as the result of photoinduced phase transition [3]–[5], which can occur on the ultrafast timescale [6]. In this paper, we will discuss recent measurements on ultrafast phase transition dynamics of correlated solids, with special emphasis on selective excitation and probing. With a focus on manganites, we will discuss how impulsive pump pulses can be tailored to achieve time-domain equivalents of filling and bandwidth control. In addition, probing techniques that address specific degrees of freedom will be presented to demonstrate the separation of different contributions to the dynamics.

## II. Manganites

Manganites are oxides of transition metals, often found in quasi-cubic perovskite structures and single- or multilayered

The work of M. Rini and R. W. Schoenlein at LBNL Materials Sciences Division and the Advanced Light Source was supported by the U.S. Department of Energy, Office of Basic Energy Sciences, Division of Materials Sciences and Engineering and the Scientific User Facilities Division respectively under Contract DE-AC02-05CH11231. The work of S. Wall was supported by the Alexander von Humboldt Foundation.

S. Wall was with the Clarendon Laboratory, University of Oxford, Oxford OX1 3PU, U.K. He is now with the Department of Physical Chemistry, Fritz Haber Institute, 14195 Berlin, Germany (e-mail: wall@fhi-berlin.mpg.de).

M. Rini was with the Materials Sciences Division, Lawrence Berkeley National Laboratory, Berkeley, CA 94720, USA. He is now with the Joint Research Centre, European Commission, Karlsruhe D-76125, Germany (e-mail: matteo.rini@ec.europa.eu).

S. S. Dhesi is with the Diamond Light Source, Harwell Science and Innovation Campus, Chilton, Didcot OX11 0DE, U.K. (e-mail: dhesi@diamond.ac.uk).

R. W. Schoenlein is with the Materials Sciences Division, Lawrence Berke- ley National Laboratory, Berkeley, CA 94720, USA (e-mail: rwschoenlein@lbl.gov).

A. Cavalleri is with the Clarendon Laboratory, University of Oxford, Oxford OX1 3PU, U.K., and also with the Max Planck Research Department for Structural Dynamics, University of Hamburg-CFEL, Hamburg 22607, Germany (e-mail: andrea.cavalleri@mpsd.cfel.de).

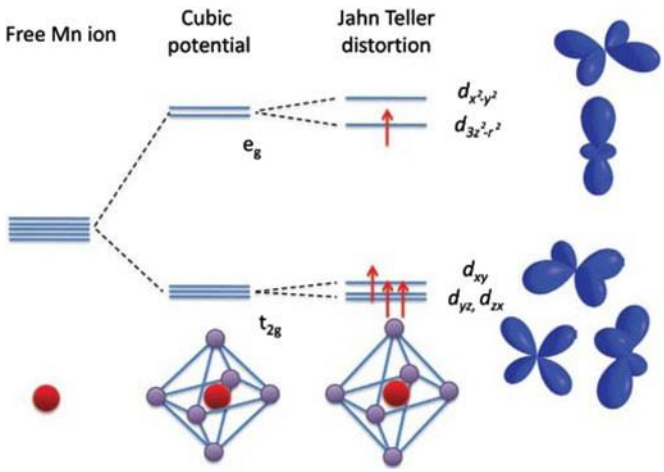


Fig. 1. Energy level diagram of the Mn ion from free space to the cubic $Mn^{4+}$ configuration and the JT distorted $Mn^{3+}$ configuration.

variations thereof. Perovskite manganites have the general formula $RE_{1-x}AE_xMnO_3$, where RE is a trivalent rare earth ion, such as La, Pr, and Nd, and AE is a divalent alkaline earth ion, such as Sr and Ca. The RE and AE ions act as charge reservoirs for the manganese ions and, by controlling the ratio of RE to AE, the average charge of the manganese ions can be continuously varied from $Mn^{3+}$ to $Mn^{4+}$. In the layered structures, the manganese centered oxygen octahedra form planes that are separated by "buffer" RE/AE layers. Manganites exhibit complex behavior, which results not only from the Mott physics described earlier, but also from the magnetic nature of the Mn-O-Mn bond, in which the sign of the exchange interaction is subtly connected to the electron transfer integral and charge distribution. This usually results in ferromagnetic conductors, while insulating phases usually occur with antiferromagnetic order. Furthermore, strong electron lattice coupling via the Jahn–Teller (JT) effect and directional exchange couplings tend to polarize the Mn orbitals along specific directions, creating superlattices of ordered orbitals. As a consequence, strong correlations between the charge, lattice, spin, and orbital parameters are found in these compounds. A large variety of phases and exotic phenomena has been observed, which has sustained the interest in these materials over the past 60 years. Such properties include charge and orbital ordering as well as many complex antiferro-magnetic and ferromagnetic spin arrangements, all of which are intricately related to the conductive or insulating properties of the material [7].

In more detail, the heart of the perovskite structure is the oxygen octahedron that surrounds the manganese ions. The field of electronegative oxygen ions results in a splitting of the otherwise degenerate, partially filled Mn 3*d* levels, resulting in a lower energy threefold degenerate $t_{2g}$ level and a higher energy $e_g$ level. The crystal field splitting in the manganites is of the order of 1 eV. Strong Hund's coupling of the Mn ion (1–2 eV) produces an alignment of the spins in the 3*d* levels. For $Mn^{4+}$ ions, this results in three spin-aligned electrons in the $t_{2g}$ level, while for $Mn^{3+}$ ions the doubly degenerate $e_g$ level is occupied by a single electron. The energy level diagram and partial crystal structure are shown in Fig. 1.

From a simple band picture, one would expect the $Mn^{3+}$ configuration to be metallic due to the partially filled $e_g$ level. However, metallicity is only found when a specific number of holes have been doped into the system, indicative of the strong electronic correlations. In addition to this, $Mn^{3+}$ ions are JT active and can reduce their energy by distorting the oxygen octahedra, introducing a strong electron–phonon interaction and an additional localization force.

Among the manganites, $Pr_{1-x}Ca_xMnO_3$ is especially interesting. The electronic hopping, which occurs between Mn ions via a bridging oxygen ion, is particularly low, due to the large Mn-O-Mn bond angle, which reduces the overlap of neighboring wavefunctions and results in a narrow electronic bandwidth. As a result, this compound shows insulating behavior at all doping $x$. However, for $x = 0.3$, the system is particularly unstable toward a competing metallic phase. From a charge and orbitally ordered antiferromagnetic insulating phase, a metallic phase can be induced by the application of magnetic fields, the CMR effect [8], electric fields [9], X-ray irradiation [10], laser irradiation [5], and pressure [11], resulting in "colossal" changes in the resistivity by up to nine orders of magnitude. Due to such intrinsic instability, $Pr_{1-x}Ca_xMnO_3$ poses an ideal testing ground for ultrafast phase-control concepts, and will be a major focus of this paper.

## III. Ultrafast Control of "Filling"

### A. Measuring the Ultrafast Photoinduced Phase Transition

Phase control by means of laser excitation is particularly interesting, both in view of potential applications and because it allows to study how changes in the long-range order, found in solids, respond to selective perturbative excitations. In order to fully understand such processes, methods are needed that can unambiguously disentangle effects arising from the different degrees of freedom, such as charge, lattice, spin, and orbital configurations.

In $Pr_{0.7}Ca_{0.3}MnO_3$, below 220 K, charge localizes in real space on the Mn ions forming an ordered network of $Mn^{3+}$ and $Mn^{4+}$ sites. This is concomitant with a real-space ordering of the directionality of electronic $e_g$ orbitals, resulting in long-range orbital order. This charge ordering prohibits electron hopping and the material is insulating. Laser excitation causes a redistribution of the charge in the material, directly perturbing the charge ordering and triggering a photoinduced phase transition [12]. This effect is often referred to as "photodoping" [13], in analogy to the filling controlled phase transition that can be achieved by chemical doping. However, photodoping opens many new possibilities, as it allows the study of changes in the charge distribution without changing the stoichiometry of the material, which often is accompanied by many unwanted concomitant effects, such as changes in the electron–phonon coupling and defect density. In addition, by using short pulses to trigger the transition, quasi-particle and transition dynamics associated with the phase transition can be observed [14].

Fig. 2 shows a direct measurement of the transient resistivity of $Pr_{0.7}Ca_{0.3}MnO_3$ after photodoping. A current amplifier was placed in series with the sample, which was held between two

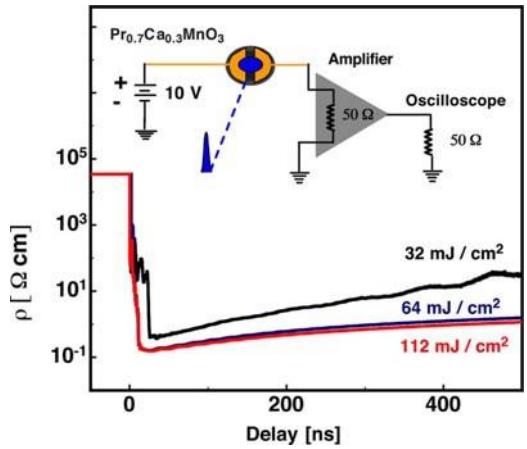


Fig. 2. Time-resolved measurement of the nanosecond resistivity transients induced by photoexcitation of $Pr_{0.7}Ca_{0.3}MnO_3$ at 77 K.

gold electrodes, 200 $\mu$m apart, deposited on the surface and biased with 10 V. After excitation with a 50 fs laser at 800 nm, a prompt resistivity drop was observed from the static value of 3.1 kΩ·cm to approximately 0.1 Ω·cm, corresponding to a conductivity change of similar magnitude as that obtained by application of a 6 T magnetic field at this temperature and doping. The photoinduced conductivity exhibits nonlinear growth with fluence and saturates above a fluence of 30 mJ/cm$^2$. Such nonlinear behavior and the long lifetime of the high-conductivity state are indicative of the destabilization of charge order and of a photoinduced phase transition.

The timescale for the resistivity measurements is limited by the bandwidth of the amplifying electronics, which results in a few nanoseconds of temporal resolution. Therefore, in order to resolve the transient dynamics, femtosecond reflectivity measurements were performed. Two independent noncollinear optical parametric amplifiers, compressed by chirped mirror pairs and driven by the same laser at 1 kHz, were used to provide independently tunable pulses in the visible spectral region [15]. The 7-fs pump pulse was tuned to a central wavelength of 550 nm in order to excite charges from O *2p* levels into the Mn *3d* $e_g$ levels. The transient reflectivity was then probed at a central wavelength of 660 nm, which could be compressed to 11 fs. $Pr_{0.7}Ca_{0.3}MnO_3$ was held in an optical cryostat with a 10-$\mu$m-thick entrance window in order to minimize dispersion on the pump and probe pulses.

Fig. 3 shows the transient change in reflectivity of $Pr_{0.7}Ca_{0.3}MnO_3$ at 77 K over timescales from 10 ps down to 400 fs. Like the transient resistivity, the transient reflectivity exhibits a long-lived response, which reaches the quasi-equilibrium of the metallic phase after a few hundred femtoseconds, with the charge and orbitally ordered antiferromagnetic phase recovering on the microsecond timescale. On zooming in to the first few picoseconds, Fig. 3(b) shows some initial dynamics: large amplitude coherent oscillation. After a background subtraction, the Fourier transform of these data over the first 2 ps shows that the central frequency of this mode is 2.38 THz (78 cm$^{-1}$). This mode has been observed in time resolved X-ray

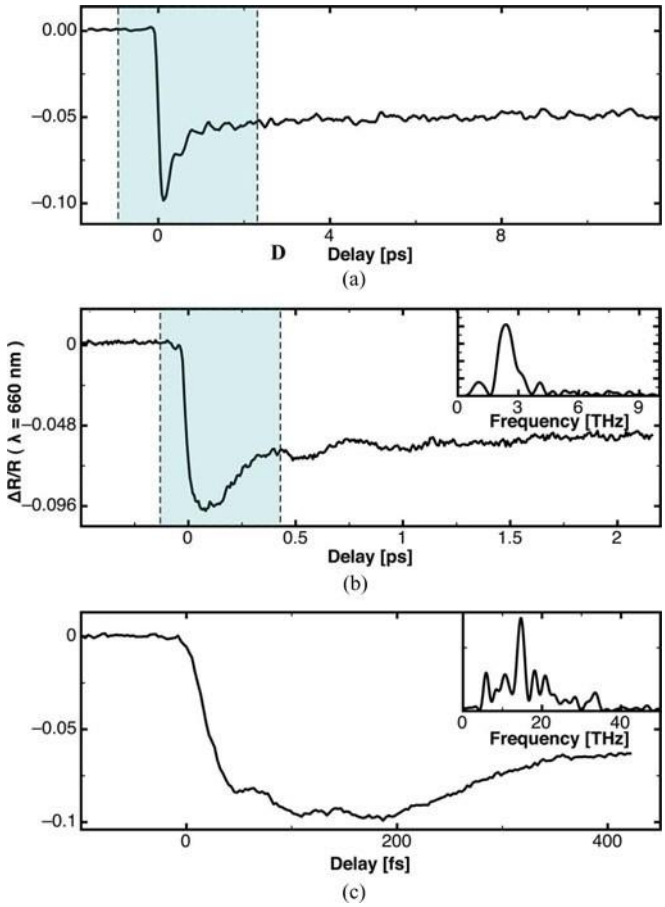


Fig. 3. Transient reflectivity during the melting of the metallic state in $Pr_{0.7}Ca_{0.3}MnO_3$ with sub-10 fs light pulses. The inserts show the Fourier transforms of the coherent response of the reflectivity.

diffraction [16], and is associated with lattice motions related with the melting of charge ordering in manganites.

On closer examination, several oscillations at a higher frequency, close to time zero, can be observed, as illustrated in Fig. 3(c). These oscillations, peaked at 14.7 THz (490 cm$^{-1}$) and persisting for 200 fs, can again be associated with phonon modes of the lattice. In this case, these modes correspond to the modulation produced by JT phonons, which are naturally triggered when charge is rapidly delocalized from JT distorted lattice sites.

These results show that lattice oscillations associated with the melting of charge order appear in the transient response of the metallic state and intricately dictate the dynamics. However, excluding the effects of the coherent lattice motion, optical measurements only demonstrate that the changes in reflectivity are rapid and persistent, but do not reveal what the actual changes to the charge distribution, and orbital and magnetic degrees of freedom are. To determine the dynamics associated with these changes, more selective probing methods are needed.

### *B. Electronic Structural Dynamics Viewed With Time-Resolved Soft X-Ray Absorption Spectroscopy*

X-ray absorption spectroscopy (XAS) is a powerful tool to probe the electronic degrees of freedom in a symmetry and

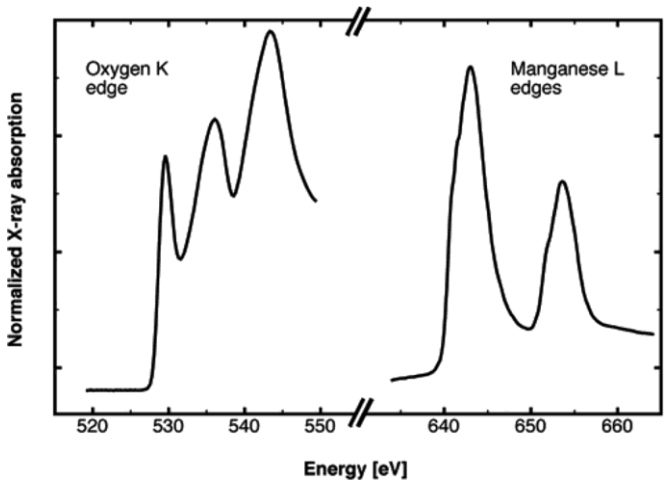


Fig. 4. Static XANES signal measured in TEY of $Pr_{0.7}Ca_{0.3}MnO_3$ at the oxygen K-edge and manganese L-edges.

element specific fashion. By measuring the energy dependence of the X-ray absorption close to a core-level transition, information about the unoccupied part of the electronic structure of a material can be obtained. This technique is referred to as X-ray absorption near edge structure (XANES) spectroscopy.

In manganites, the relevant electronic states close to the Fermi level arise from the hybridization of Mn-3*d* and O-2*p*states, which contribute to form valence and conduction bands that dominate the electronic properties of the system. XANES measurements in the spectral regions of the O K-edge and Mn L-edges probe unoccupied states of O-2*p* and Mn-3*d* character, respectively, and can thus provide complementary information on rearrangements of electronic states of different sym metry. The metal–insulator phase transition produced characteristic changes of the XANES signal at both the O K- and Mn L-edges [17], [18], reflecting the collapse of the insulating bandgap and the modification in JT distortions [19]. By extend ing XANES spectroscopy to the time domain, new and specific information about the rearmament of the electronic structure as a function of time can be obtained [20], [21].

Fig. 4 shows the static XANES signal of $Pr_{0.7}Ca_{0.3}MnO_3$ at the oxygen K-edge and manganese L-edge. Measurements were taken at 80 K at the 4-ID-C undulator beamline at the Advanced Photon Source, Argonne National Laboratory and measured in total electron yield (TEY). The XANES spectra around the oxygen K-edge probe electronic transitions from the O-1*s* level to O-2*p* unoccupied levels around the Fermi level and to the continuum. Three preedge peaks are clearly observed at 529.6, 536.1, and 543.3 eV, before the transitions into the vacuum. These peaks correspond to transitions to oxygen 2*p* levels that are strongly hybridized with the wavefunctions of neighboring ions. The most interesting peak for revealing changes in the electronic structure is the lowest energy peak, which corresponds to transitions to 2*p* levels hybridized with the Mn 3*d* levels, whereas the other peaks corresponds to hybridization with the Pr 5*d*/Ca 3*p* and Mn 4*sp*-hybridized levels, respectively [22]. Previous static studies in related manganites have focused on

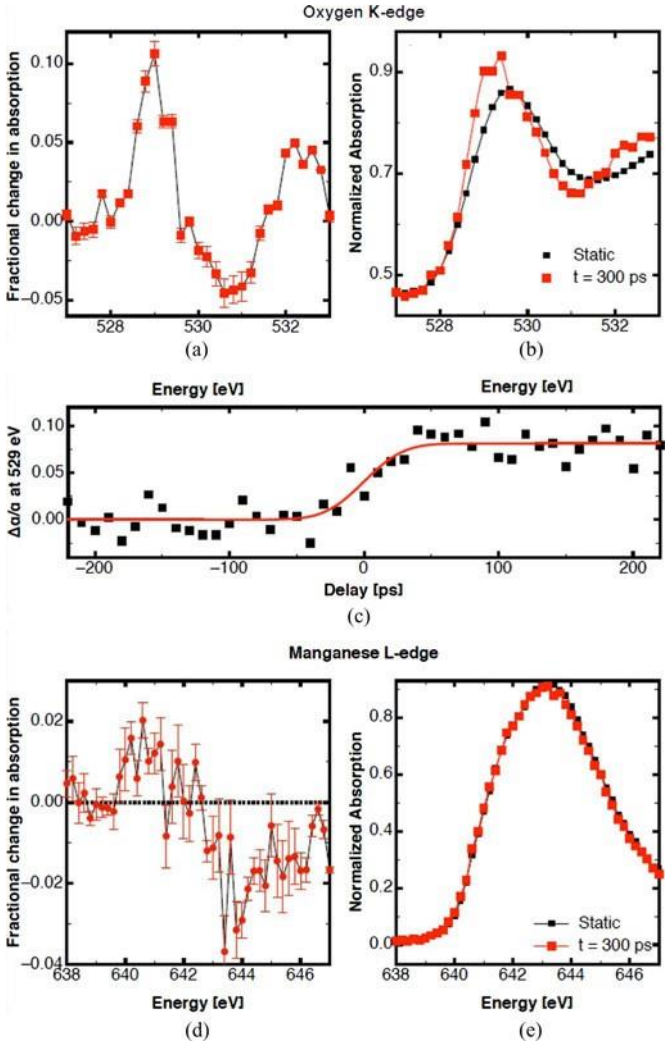


Fig. 5. (a) Fractional change in XANES signal at the first oxygen preedge 300 ps after excitation. (b) Oxygen preedge before and after excitation. (c) Time-resolved scan on the dynamics measured at 529 eV. (d) Fractional change in XANES signal at the Mn $L_{III}$ 300 ps after excitation. (e) Mn $L_{III}$ before and after excitation.

changes at the 529.6 eV O preedge, identifying unambiguous signatures of the insulator–metal phase change in this spectral region [18], [19]. On the other hand, Mn L-edge measurements probe transitions from the spin-orbit split $L_{II}$ - and $L_{III}$ -edge into unoccupied 3*d* levels. Static temperature-dependent L-edge experiments in the literature have shown subtle changes at the Mn L-edge upon the phase transition [17]. It has been shown that, while the O K-preedge can be seen as a direct mapping of the density of unoccupied states [23], the interpretation of Mn L-edge spectra is less straightforward and has to take into account strong core–hole renormalization and multiplet effects [24].

Fig. 5 summarizes the results from time-resolved XANES experiments at the oxygen and manganese edges. XANES spectra exhibit a clear and large photoinduced effect, which reflects rearrangements of the electronic structure that are indicative of an electronic phase transition [25].

The time-resolved XANES experiments were performed at beamline 6.0.1 at the Advanced Light Source, Lawrence

Berkeley National Laboratory in ultra high vacuum (UHV) conditions. The sample, cooled to 80 K, was excited by a 1 kHz, 50 fs, 800 nm Ti:Sapphire laser, focused to 20 mJ/cm$^2$, which was electronically synchronized to the synchrotron. Fig. 5(a) and (d) shows this relative change in the XANES signal at the first oxygen preedge and the manganese $L_{III}$ edge, respectively, while Fig. 5(b) and (e) shows the absolute signal. Both measurements were performed 300 ps after laser excitation, when the material is in the metastable metallic phase.

These experiments had a time resolution of 70 ps, as demonstrated in the time scan of transient response of the system at 529 eV. From these data, several important points can be obtained from the observed changes at the O K- and Mn L-edges. First, these data reveal that the long-lived product state cannot be due to a trivial laser-heating effect, as photoinduced changes of XANES spectra exhibit a different behavior from those observed over a broad temperature range of $Pr_{0.7}Ca_{0.3}MnO_3$. It is worth noting that, as a consequence of its narrow electronic bandwidth, $Pr_{0.7}Ca_{0.3}MnO_3$ remains insulating at all temperatures [8]. Further, the dynamics of time-resolved XANES spectra can be directly connected to specific rearrangements of the density of states across the insulator–metal transition.

As the metallic state is formed and the insulating bandgap collapses the density of unoccupied $e_g$ states in the conduction band changes, building up near the Fermi level. Since the oxygen K-edge, is hybridized with the unoccupied electronic Mn *d*-states close to the Fermi level, this results in a transfer of spectral weight to the preedge absorption threshold for oxygen. The shift observed here shows a remarkably similar trend to those observed in other CMR manganites, which *do* exhibit a temperature-driven insulator to metal transition at the Curie temperature ($T_C$), including $La_{0.7}Sr_{0.3}MnO_3$ ($T_C = 360$ K), and $Pr_{0.7}Sr_{0.3}MnO_3$ ($T_C = 250$ K), and the double-layered compound $La_{1.3}Sr_{0.7}Mn_2O_7$ ($T_C = 130$ K) (18). This observation further strengthens the link between the photoinduced shift of spectral weight at the O K-edge and the occurrence of an insulator–metal transition. In addition, small changes are also observed at the Mn L-edges.

By directly monitoring the temporal evolution of the density of unoccupied states close to the Fermi level, XANES spectroscopy reveals the formation of the metallic state electronic structure, characterized by a shift in spectral weight toward lower energies. These shifts share many similarities to thermodynamic phase transitions in similar manganites. In those compounds, metallicity is concurrent with a change in magnetic state. Therefore, in the following section, we discuss progress toward realizing measurements of the temporal evolution of the spin and orbital subsystem directly.

### *C. Ultrafast Probing of Magnetic and Orbital Ordering*

So far we have used transient reflectivity measurements to show that the transition to the metallic state occurs on an ultrafast timescale and by using XAS, we have shown how this results in changes in electronic distribution around the Fermi level. These transitions occur from initial states that possessed long range orbital and magnetic ordering. Therefore, it is important to address how these parameters respond to photoexcitation. These orderings can be directly probed by measuring the periodicity along certain crystallographic directions. For the manganites, this is particularly challenging because the probe must be sensitive to fractional changes in valence charge that varies periodically on a few nanometer length scale.

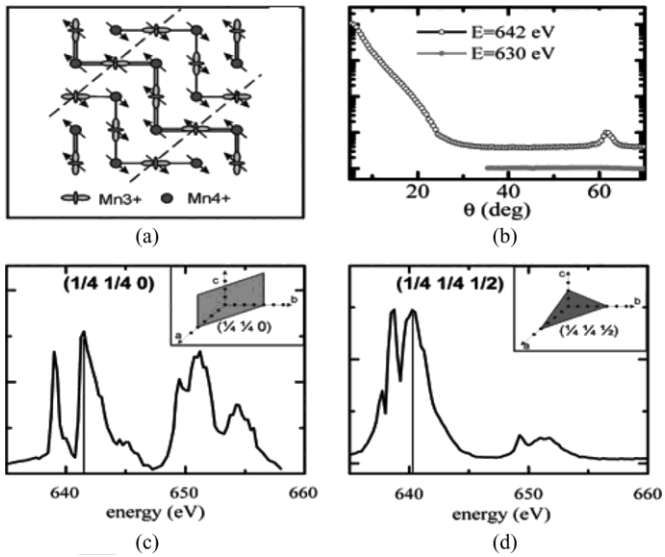


Fig. 6. (a) Schematic representation of the charge spin and orbital ordering found in $La_{0.5}Sr_{1.5}MnO_4$. (b) Soft X-ray reflected intensity of $La_{0.5}Sr_{1.5}MnO_4$ on and off resonance (log scale). At 62°, the peak of the superlattice reflection resulting from the orbital ordering is observed, only for energies resonant with the Mn L-edges. The angular independent background is the result energy dependent fluorescence of the sample, which is emitted into all angles. (c) and (d) Energy-resolved scans of the $(\frac{1}{4}, \frac{1}{4}, 0)$ orbital ordering and $(\frac{1}{4}, \frac{1}{4}, \frac{1}{2})$ antiferromagnetic ordering peaks.

To achieve this sensitivity, we use resonant soft X-ray diffraction and extend it to the time domain. In this paper, we study the single-layered manganite $La_{0.5}Sr_{1.5}MnO_4$ as the charge and orbital ordering is commensurate with the lattice. Below $T_{COO/CO} = 220$ K, $La_{0.5}Sr_{1.5}MnO_4$ adopts an in-plane charge ordering in which $Mn^{3+}$ and $Mn^{4+}$ ions for a "checker-board" type pattern [26]. At the same time, the orientation of the $e_g$ orbitals on the $Mn^{3+}$ sites order in zig-zag chains, as shown in Fig. 6(a). Below $T_N = 110$ K, antiferromagnetic spin ordering of the CE-type (ferromagnetic spin alignment along the zig-zag orbital chains which are antiferromagnetically coupled within the *ab*-plane and antiferromagnetic ordering along the *c*-axis) also occurs. When X-rays are resonant with the manganese L-edges soft X-ray diffraction become sensitive to the charge and orbital ordering due to virtual transitions to the unoccupied Mn 3*d* states, which are different for $Mn^{3+}$ and $Mn^{4+}$ ions. This contrast results in a superlattice peak at the Bragg scattering angle of an enlarged unit cell. Fig. 6(b) shows one such peak, which corresponds to scattering from the (1/4, 1/4, 0) planes, reflecting the orbital order observed in the system. This peak is absent off resonance as there is no contrast mechanism to distinguish the lower symmetry state.

In addition to the orbital order peak, scattering from the (1/4, 1/4, 1/2) plane is sensitive to the magnetic structure of the

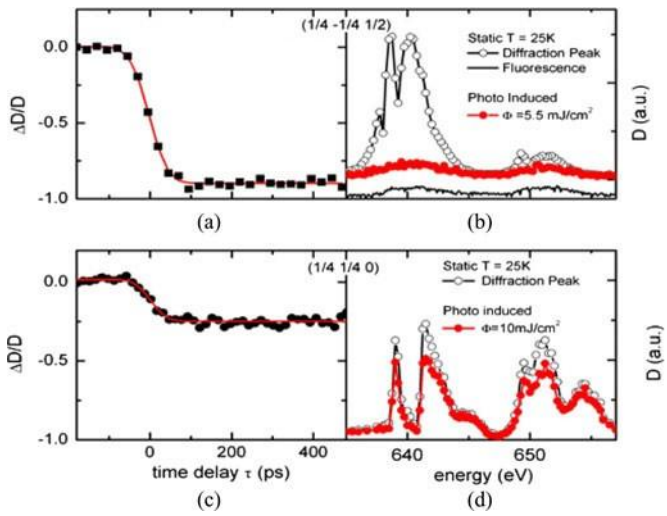


Fig. 7. (a) Time-resolved changes in diffraction intensity at 640.25 eV and (b) energy-resolved diffraction signal before and 200 ps after laser excitation, for the $(\frac{1}{4}, \frac{1}{4}, \frac{1}{2})$ magnetic diffraction peak. (c) Time-resolved changes in diffraction intensityat 641.5 eV and (d) energy-resolved diffraction signal before and 200 ps after laser excitation, for the $(\frac{1}{4}, \frac{1}{4}, 0)$ orbital diffraction peak.

material [27], thus enabling a separation of charge orbital dynamics from the spin dynamics. Fig. 6(c) and (d) shows the energy dependence of the orbital and magnetic peaks, respectively. By analyzing the energy dependence, the driving forces behind long range ordering can be obtained [28]. By following the dynamics of these peaks in the time domain, it is possible to separately track the evolution of both the magnetic and orbital degrees of freedom in the system.

Time-resolved measurements of the diffraction intensity of each peak were performed at beamline IO6 (Diamond Light Source). The sample was excited with an 800-nm laser source at 20 kHz, synchronized to the synchrotron storage ring, and the diffraction peak was measured using a multichannel plate and gated discriminator to provide single photon sensitivity. The orbital ordering peak was measured with a sample cut with a (1 1 0) surface, and the magnetic peak was measured on a sample with a (1 1 2) surface. Both samples were cooled with liquid helium to 25 K, well below both the antiferromagnetic and orbital ordering temperatures.

Fig. 7 shows the transient response of the magnetic (1/4, 1/4, 1/2) and orbital (1/4, 1/4, 0) peaks, together with energy resolved scans of these diffraction peaks 200 ps after excitation. For all excitation fluences above 5 mJ/cm$^2$, the magnetic (1/4, 1/4, 1/2) peak entirely vanishes, leaving only a weak signal due to the energy-dependent background fluorescence. In contrast, the photoinduced reduction in the orbital (1/4, 1/4, 0) scattering is lower, even for excitation with 10 mJ/cm$^2$. Again, the transient response of the system is limited to the 70 ps duration of the X-ray bunch; however, additional measurements made with 10 ps pulses, when the synchrotron was operating in the low-alpha mode, showed no additional dynamics. Therefore, on these timescales, we can conclude that photoexcitation exhibits a greater perturbation to the spin ordering than the in-plane orbital ordering.

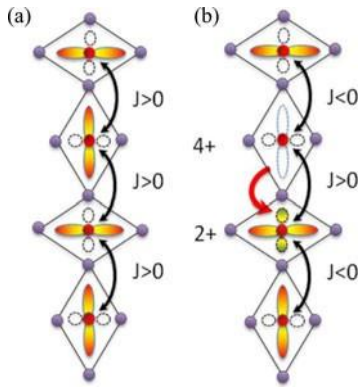


Fig. 8. (a) JT distortion within the *ab*-plane and occupied–unoccupied bond overlap giving rise to the ferromagnetic in-plane exchange interaction. (b) State of the system after photoexcitation, demonstrating how the GK rules applied to the excited state can change the sign of the exchange interaction.

### *D. Dynamic Magnetoelastic Coupling*

In the previous sections, we demonstrated the progress that has been made toward measuring the ultrafast structural, electronic, orbital, and spin rearrangements that occur during the photoinduced phase transition of the manganites. However, several outstanding issues remain. For example, the transition to a metallic phase of $Pr_{0.7}Ca_{0.3}MnO_3$ is usually accompanied by a transition of the spin subsystem to ferromagnetic order. This has been observed in other manganites [29], yet the mechanism by which a light pulse can ultimately lead to a change in magnetic state in these materials remains unknown. More fundamentally, the mechanisms that ultimately couple the photon to rearrangements in the charge, spin, lattice, and orbital degrees of freedom are poorly understood.

In order to investigate this coupling, we studied the mechanism of coherent phonon generation in the parent compound $LaMnO_3$. This material retains many essential features and the complexity of the doped manganites, while not exhibiting CMR or a photoinduced phase transitions, normally only found in doped compounds. In addition, difficulties associated with phase separation [30] are not present, and a clearer picture of the microscopic physics can be gained from optical measurements. By using sub-10 fs pulses of light, we are able to resolve coherent motion of the lattice at frequencies up to 20 THz [31].

In $LaMnO_3$, below 780 K, a cooperative JT distortion of the oxygen octahedra within the *ab*-planes lifts the degeneracy of the $e_g$ levels and gives rise to a staggered orbital structure. Below 140 K, $LaMnO_3$ adopts an A-type antiferromagnetic spin ordering, in which spins are aligned ferromagnetically within the *ab*-planes, and antiferromagnetically along the *c*-axis. This ordering, shown along the *a*-axis in Fig. 8(a), can be intuitively explained by applying the Goodenough–Kanamori (GK) rules to the crystal structure [32].

According to the GK rules, the exchange integral *J*, will be negative, i.e., prefer antiferromagnetic alignment, if the bonding between two Mn ions is formed between two half-filled orbitals or between two empty orbitals. This is because virtual hopping between two $e_g$ orbitals through the bridging oxygen $2p$ orbitals is constrained by the Pauli exclusion principle. If

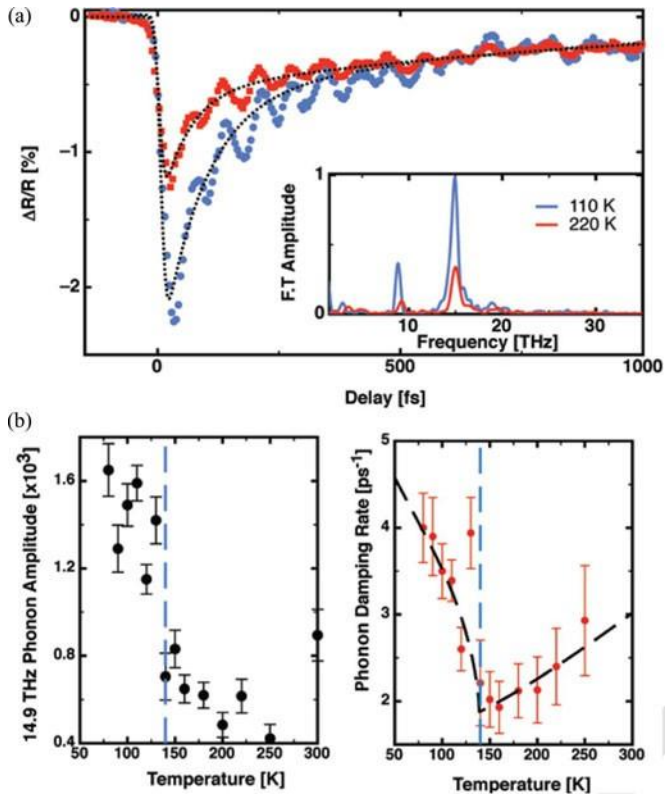


Fig. 9. (a) Transient reflectivity of $LaMnO_3$ above and below the antiferromagnetic ordering temperature. The insert shows the Fourier transform of the oscillations, clearly showing two phonon modes are present at 14.9 THz (497 $cm^{-1}$) and 8.8 THz (293 $cm^{-1}$). (b) Temperature dependence of the amplitude (left) and damping rate (right) of the 14.9 THz mode. The dashed Verticle line marks the Neel temperature.

the bond is between a half-filled orbital and an empty orbital or between a filled orbital and a half-filled orbital, hopping is constrained by Hund's rule, and the exchange integral is positive, favoring ferromagnetic order. Furthermore, bonds that have an antifer-romagnetic exchange interaction are shorter than those with a ferromagnetic interaction due to stronger covalent bonding. In $LaMnO_3$, the static JT distortion within the *ab*-plane leads to overlap between half-filled $e_g$ $3d_{az^2-r^2}$ orbitals and empty $e_g$ $3d_{x^2-y^2}$ orbitals resulting in a positive exchange integral. Along the *c*-axis, the bonding is dictated by the half-filled $t_{2g}$ levels, resulting in antiferromagnetic coupling between the planes.

For these experiments, the excitation energy was tuned to the inter-Mn charge transfer resonance at 1.9 eV, which corresponds to a charge transfer from $2Mn^{3+}$ ($t^a_{2g\uparrow e_g\uparrow}$) to $Mn^{4+}$ ($t^3_{2g\uparrow}$), $Mn^{2+}$ ($t^a_{2g\uparrow e^2_g\uparrow}$). Probing was performed at 2.2 eV, so that color filters could be used to reduce the detection of scattered light. Fig. 9(a) shows the transient response of $LaMnO_3$ above and below the antiferromagnetic ordering temperature. Unlike $Pr_{0.7}Ca_{0.3}MnO_3$, a long-lived metastable state is not observed as no insulator-to-metal phase transition occurs. Instead large amplitude and persistent oscillations are seen.

The Fourier transform of these data show that two modes are present in the oscillations. These modes correspond to the JT stretching at 14.9 THz (497 $cm^{-1}$), as observed in $Pr_{0.7}Ca_{0.3}MnO_3$, and a JT bending mode at 8.8 THz (293 $cm^{-1}$) [33]. The amplitude and damping rate of the stronger, JT stretching mode is followed as a function of temperature in Fig. 9(b). The frequency of each mode remained constant at all temperatures. Above the transition temperature, the amplitude of the phonon mode remains approximately constant. In addition to this, the damping rate of the oscillation is well described by anharmonic decay into two acoustic phonons with equal energy and opposite momentum, which becomes less likely for decreasing temperatures and reduces the damping rate.

On crossing the transition temperature, a sharp change in both the amplitude and the damping rate are observed. A step-like increase occurs in the amplitude of the oscillations and this is accompanied by a sudden increase in the damping rate. This damping rate increases with the increasing magnetization of the sample and is indicative of a new scattering channel for the phonons. This new channel corresponds to the scattering of phonons by magnons.

This increase can be explained by applying the GK rules to the excited state of the system. The charge transfer excitation at 1.9 eV creates $Mn^{4+}$ and $Mn^{2+}$ pairs. These states are no longer JT active and create the large amplitude JT oscillations. In addition, the excitation also modifies the bonding between the manganese and oxygen ions. Bonds between neighboring Mn ions in the *ab*-plane also consist of half-filled to half-filled and empty-to-empty bonding [see Fig. 8(b)], which prefer a negative exchange, and therefore, perturb the local magnetic ordering. This change in exchange not only provides the coupling to the lattice vibrations to the magnons, but also drives changes in the equilibrium bond lengths, which results in the higher amplitude excitation.

## IV. Ultrafast Control of Bandwidth

The previous sections described how lattice, orbital, and spin configurations of manganites are mutually coupled and related to charge transfer excitations. The fact that these strong couplings exist raises the intriguing possibility that direct lattice excitation may drive a similar effect, while the material remains in its electronic ground state. In the following, we show that direct excitation of IR-active phonon modes provides a dynamical way to exert bandwidth control on a correlated-electron material.

In manganites with a perovskite structure, a key parameter for the description of the relationship between structural and electronic properties is the geometrical "tolerance factor" Γ [34], defined as follows:

$$\Gamma = \frac{(A - O)}{\sqrt{2}\,(Mn - O)}$$

which depends on the average A–O (A = Pr, Ca, La, Sr,...) and Mn–O distances. Γ quantifies the degree of orthorhombic distortion from an ideal cubic perovskite symmetry and is microscopically related to the Mn–O–Mn bond angle ($\theta$), and hence, to orbital overlap and to the transfer integral *t* describing electron hopping between $Mn^{3+}$ and $Mn^{4+}$ sites. The hopping matrix element is maximum for Γ = 1 (cubic structure, $\theta = 180^\circ$), where metallic behavior is expected, and decreases for smaller angles

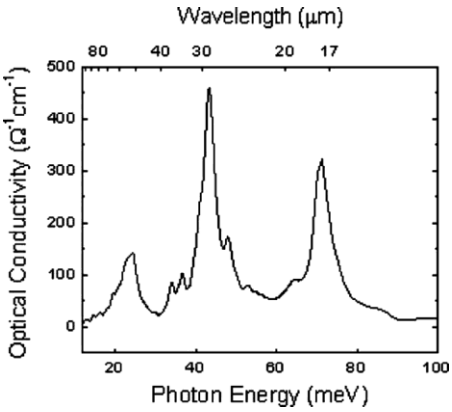


Fig. 10. Optical conductivity spectrum of $Pr_{0.7}Ca_{0.3}MnO_3$ at low temperature (10 K). The highest frequency mode at 17 $\mu$m is assigned to the Mn–O stretching vibration, which modulates the Mn–O distance, and hence, the tolerance factor.

($\Gamma < 1$, $\theta < 180^{\circ}$), as is the case for symmetry-lowering orthorhombic distortions associated with a compression of the Mn–O–Mn bond and an elongation of the A–O bond [35]. Through the connection with the transfer integral, the tolerance factor has been shown to control the magnetic and electronic properties of manganites, including the magnitude of the CMR effect and the metal–insulator transition temperature [11], [36]. A universal phase diagram as a function of temperature and tolerance factor has been derived for $A_{0.7}A^{t}_{0.3}MnO_3$ systems, showing that such materials can be driven across the boundaries of ferromagnetic insulator, ferromagnetic metal, and paramagnetic insulator phases by very subtle changes in tolerance factor. Such a direct and sensitive coupling between geometrical parameters and the electron transfer integral is exploited in conventional static strategies for "bandwidth-control," in which the one-electron bandwidth $W$ ($\propto t$) is finely tuned by tolerance factor modifications, as obtained by application of hydrostatic pressure or by variation of the ionic size of the rare-earth atom at the A site of the perovskite structure.

Resonant vibrational excitation can be applied to impulsively modulate the tolerance factor, providing a testing route for ultrafast bandwidth-control strategies. Excitation of IR-active phonon modes can be used to perturb the lattice, changing bond angles and distances in a selective fashion. This modifies the overlap of neighboring electronic wavefunctions and the asso ciated electron hopping probability. Here, we prove this concept on the magnetoresistive manganite $Pr_{0.7}Ca_{0.3}MnO_3$, where direct excitation of a phonon mode at 71 meV (17 $\mu$m) leads to an ultrafast insulator–metal electronic phase transition. Unlike previous below-gap excitations, the electronic degree of freedom remains unperturbed [37].

The optical conductivity spectrum of $Pr_{0.7}Ca_{0.3}MnO_3$ shown in Fig. 10 exhibits a three-peak structure that is characteristic of most quasi-cubic perovskites [38]. The highest frequency IR active mode at 17 $\mu$m corresponds to a Mn–O stretching vibration, which modulates the geometrical parameters determining the tolerance factor $\Gamma$ and is thus expected to be strongly coupled to the electron system. Intense and tunable femtosecond pulses at this wavelength can be generated by difference

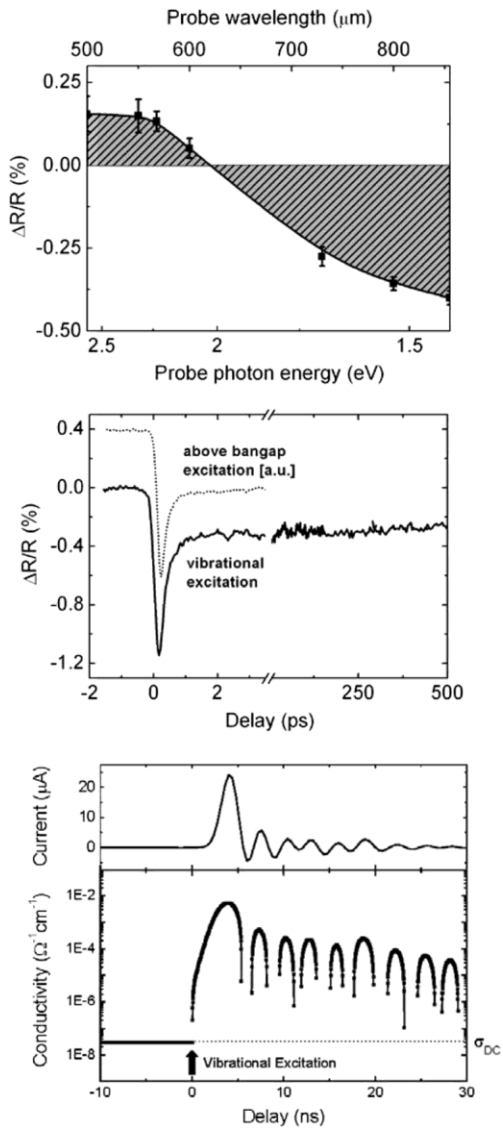


Fig. 11. (a) Relative change of reflectivity ($\Delta R/R$) as a function of probe frequency measured 1 ps after vibrational excitation at 17 $\mu$m. (b) Transient $\Delta R/R$ at 800 nm as a function of pulse delay following vibrational excitation (solid line) and optical excitation at 800 nm (dotted line). (c) Time-dependent transport measurement show a 1000-fold increase in the sample current (upper panel) and a $\sim 10^5$ increase in sample conductivity (lower panel) following vibrational excitation of the Mn–O stretching mode.

frequency generation between signal and idler of an IR optical parametric amplifier [39]. We investigated the response of $Pr_{0.7}Ca_{0.3}MnO_3$ to resonant impulsive excitation of the 17 $\mu$m mode by means of two experimental approaches: 1) the ultrafast formation of a metallic-like reflectivity spectrum at visible-to-IR wavelengths was observed by ultrafast mid-IR-pump/optical-probe spectroscopy and 2) a prompt, five-order-of-magnitude drop in resistivity following vibrational excitation is established by transient conductivity measurements.

Ultrafast pump-probe experiments on $Pr_{0.7}Ca_{0.3}MnO_3$ single crystals at 30 K measure the transient sample reflectivity following resonant excitation by mid-IR pulses. Fig. 11(a) shows the relative reflectivity change $(\Delta R/R)$ as a function of

frequency measured 1 ps after 17 $\mu$m excitation. Excitation by photons at 70 meV energy (17 $\mu$m) results in modifications of the reflectivity spectrum at electronvolt energies. Characteristic signatures of the formation of a metallic state are observed, deriving from the collapse of the 0.3 eV insulating gap and the formation of a pseudoplasma edge in the metallic state [40]. Fig. 11(b) shows the reflectivity dynamics at 800 nm following vibrational excitation, revealing that the vibrationally induced phase is formed within the 300-fs experimental resolution and is metastable, with a lifetime extending into the nanosecond range. The pump-fluence threshold for inducing such reflectivity changes is dramatically enhanced upon resonant excitation of the Mn–O stretching vibration [39]. The specificity of the Mn–O vibration may be assessed in the future by comparing with excitation of lower energy phonon modes, once intense sources of terahertz pulses become available in this spectral region.

Measurements of the sample resistance following mid-IR excitation allowed the assessment of the transient conduction properties of the sample. Laser pulses at 17 $\mu$m were used to excite the sample, with the laser spot fully covering a 200-$\mu$m gap between two biased electrodes. The sample current was monitored by electronics with a 4-ns temporal resolution. Experiments were carried out at 30 K, with the sample in the charge-ordered, antiferromagnetic insulating phase. Following mid-IR excitation, a 1000-fold increase in sample current was observed, as shown in Fig. 11(c) (upper panel). Fig. 11(c) (lower panel) shows the corresponding increase of sample conductivity derived from the measured transient current by assuming a uniform transition to the conductive state throughout the excited sample volume. From this, a dramatic, five-order-of-magnitude jump of sample conductivity, from $\sim 3 \times 10^{-8}\ \Omega^{-1}\cdot\mathrm{cm}^{-1}$ to at least $\sim 5 \times 10^{-3}\ \Omega^{-1}\cdot\mathrm{cm}^{-1}$, is estimated. The metastable metallic phase is formed and relaxes within the experimental time resolution and the sample recovers its original resistance within several tens of nanoseconds. At the photon energy and laser fluence used in these measurements, both interband carrier excitations and laser heating effects can be ruled out as the origin of this resistivity drop.

Our results demonstrate that the selective and coherent excitation of the Mn–O phonon mode results in an ultrafast transition to a metastable, high-conductivity phase of $Pr_{0.7}Ca_{0.3}MnO_3$. Since no electronic excitation is involved, this strongly suggests that the origin of such a remarkable behavior lies in the impulsive modulation of the "tolerance factor," allowing for the ultrafast control of the 1-electron bandwidth and hence of the electronic phase of correlated solids. This has recently been demonstrated in the layered compound $La_{0.5}Sr_{1.5}MnO_4$, where selective excitation has been used to melt orbital ordering [41]. Similar strategies may provide important new insights into the coupling between low-energy excitations and electronic structures of complex solids.

## V. Summary and Outlook

This paper has shown how pump and probe ultrafast spectroscopy can be used to unravel the complex dynamics that underpin the physics of correlated materials. We have demonstrated how specific probes enable the selective investigation of one of many coupled degrees of freedom. In particular, soft X-ray techniques have been used to separate charge, spin, and orbital dynamics in manganites. Future studies will focus on extending these techniques to study the initial dynamics on timescales, currently only achievable with optical probes. This will enable direct observation of the coupling and energy flow between competing order parameters. Given the high photon-number requirements, these experiments are unfeasible with current short pulse X-ray sources [42]. However, with the growth of new and tunable short-pulse X-ray sources, such as free electron lasers (FELs) and high-harmonic sources [43], we anticipate that these techniques will provide significant contributions to the understanding of dynamics in these materials.

In addition, we have shown that by tuning the wavelength of coherent excitation pulses, temporal analogies to filling and bandwidth control can be achieved, manipulating the materials on ultrafast timescales and enabling new forms of control over condensed phase materials. The combination of selective excitation techniques with selective probes will surely provide a challenge. Yet this would enable a full comparison of the two regimes and offer a greater insight into the processes responsible for phase control.

Finally, the probing region can be further expanded to measure the low frequency response of the system with terahertz spectroscopy [44], [45]. Further changes in the Fermi surface can be measured with time-resolved photoemission spectroscopy [46], [47], while changes in the structural ordering can be followed with femtosecond hard X-ray diffraction [48] or electron diffraction [49]. The combination of all these techniques will provide unprecedented insights into ultrafast dynamics and phase transitions, and may result in new ideas for controlling and manipulating properties of complex solids.

## Acknowledgment

This paper would not have been possible without the contributions of H. P. Ehrke, University of Oxford, R. I. Tobey, Brookhaven National Laboratory, Y. Zhu, Lawerence Berkeley, National Laboratory, and G. Cerullo, Politecnico di Milano, Italy. The authors would like to thank A. T Boothroyd, University of Oxford, and Y Tokura, AIST, Japan.

## References

[1] N. F. Mott, "Metal-insulator transition," *Rev. Mod. Phys.*, vol. 40, pp. 667–683, 1968.

[2] M. Chollet, L. Guerin, N. Uchida, S. Fukaya, H. Shimoda, T. Ishikawa, K. Matsuda, T Hasegawa, A. Ota, H. Yamochi, G. Saito, R. Tazaki, S. Adachi, and S. Koshihara, "Gigantic photoresponse in 1/4-filled-band organic salt (EDO-TTF)$_2$PF$_6$," *Science*, vol. 307, pp. 86–89, 2005.

[3] S. Koshihara, Y. Tokura, T. Mitani, G. Saito, and T. Koda, "Photoinduced valence instability in the organic molecular compound tetrathiafulvalene-p-chloranil (TTF-CA)," *Phys. Rev. B*, vol. 42, pp. 6853–6856, 1990.

[4] A. Cavalleri, M. Rini, and R. W. Schoenlein, "Ultra-broadband femtosecond measurements of the photo-induced phase transition in $VO_2$: From the mid-IR to the hard X-rays," *J. Phys. Soc. Jpn*, vol. 75, p. 011004, 2007.

[5] K. Miyano, T. Tanaka, Y. Tomioka, and Y. Tokura, "Photoinduced insulator-to-metal transition in a perovskite manganite," *Phys. Rev. Lett.*, vol. 78, pp. 4257–4560, 1997.

[6] A. Cavalleri, Th. Dekorsy, H. Chong, J. C. Kieffer, and R. W. Schoenlein, "Evidence for a Structurally Driven Insulator-to-metal transition in $VO_2$: A view from the ultrafast timescale," *Phys. Rev. B*, vol. 70, p. 161102(R), 2004.

[7] M. V. Zimmermann, J. P. Hill, D. Gibbs, M. Blume, D. Casa, B. Keimer, Y. Murakami, Y. Tomioka, and Y. Tokura, "Interplay between charge, orbital, and magnetic order in $Pri_{1-x}Ca_xMnO_3$," *Phys. Rev. Lett.*, vol. 83, pp. 4872–4875, 1999.

[8] Y. Tomioka, A. Asamitsu, H. Kuwahara, Y. Moritomo, and Y. Tokura, "Magnetic-field-induced metal-insulator phenomena in $Pri_{1-x}Ca_xMnO_3$ with controlled charge-ordering instability," *Phys. Rev. B*, vol. 53, pp. R1689–R1692, 1996.

[9] A. Asamitsu, Y. Tomioka, H. Kuwahara, and Y. Tokura, "Current switching of resistive states in magnetoresistive manganites," *Nature*, vol. 388, pp. 50–52, 1997.

[10] V. Kiryukhin, D. Casa, J. P. Hill, B. Keimer, A. Vigliante, Y. Tomioka, and Y. Tokura, "An X-ray-induced insulator-metal transition in a magnetoresistive manganite," *Nature*, vol. 386, pp. 813–815, 1997.

[11] H. Y. Hwang, T. T. M. Palstra, S. W. Cheong, and B. Batlogg, "Pressure effects on the magnetoresistance in doped manganese perovskites," *Phys. Rev. B.*, vol. 52, pp. 15046–15049, 1992.

[12] M. Fiebig, K. Miyano, Y. Tomioka, and Y. Tokura, "Visualization of the local insulator-metal transition in $Pr_{0.7}Ca_{0.3}MnO_3$," *Science*, vol. 280, pp. 1925–1928, 1998.

[13] G. Yu, C. H. Lee, A. J. Heeger, N. Herron, and E. M. McCarron, "Transient photoinduced conductivity in single crystals of $YBa_2Cu_3O_6$ : 'Photodoping' to the metallic state," *Phys. Rev. Lett.*, vol. 67, pp. 2581–2584, 1991.

[14] D. Polli, M. Rini, S. Wall, R. W. Schoenlein, Y. Tomioka, Y. Tokura, G. Cerullo, and A. Cavalleri, "Coherent orbital waves in the photo-induced insulator-metal dynamics of a magnetoresistive manganite," *Nat. Mat.*, vol. 6, pp. 643–647, 2007.

[15] C. Manzoni, D. Polli, and G. Cerullo, "Two-color pump–probe system broadly tunable over the visible and the near infrared with sub-30 fs temporal resolution," *Rev. Sci.*, vol. 77, p. 023103, 2006.

[16] P. Beaud, S. L. Johnson, E. Vorobeva, U. Staub, R. A. De Souza, C. J. Milne, Q. X. Jia, and G. Ingold, "Ultrafast structural phase transition driven by photoin-duced melting of charge and orbital order," *Phys. Rev. Lett.*, vol. 103, p. 155702, 2009.

[17] O. Toulemonde, F. Millange, F. Studer, B. Raveau, J.-H. Park, and C.-T. Chen, "Changes in the Jahn–Teller distortion at the metal– insulatortransition in CMR manganites $(Pr, Nd)_{0.7}(Sr, Ca)_{0.3}MnO_3$," *J. Phys. Condens. Matter*, vol. 11, pp. 109–120, 1999.

[18] J.-H. Park, T. Kimura, and Y. Tokura, "Competition between lattice distortion and charge dynamics for the charge carriers of double-layered manganites," *Phys. Rev. B.*, vol. 58, pp. R13330–R13333, 1998.

[19] N. Mannella, A. Rosenhahn, M. Watanabe, B. Sell, A. Nambu, S. Ritchey, E. Arenholz, A. Young, Y. Tomioka, and C. S. Fadley, "Temperature-dependent x-ray absorption spectroscopy of colossal magnetoresistive perovskites," *Phys. Rev. B*, vol. 71, p. 125117, 2005.

[20] A. Cavalleri, H. H. W. Chong, S. Fourmaux, T. E. Glover, P. A. Heimann, J. C. Kieffer, B. S. Mun, H. A. Padmore, and R. W. Schoenlein, "Picosecond x-ray absorption measurement of the photo-induced insulator-to-metal transition in $VO_2$," *Phys. Rev. B.*, vol. 69, p. 153106, 2004.

[21] A. Cavalleri, M. Rini, H. H. W. Chong, S. Fourmaux, T. E. Glover, P. A. Heimann, J. C. Kieffer, and R. W. Schoenlein, "Band-selective measurement of electronic dynamics in $VO_2$ with femtosecond NEXAFS," *Phys. Rev. Lett.*, vol. 95, p. 067405.

[22] M. Abbate, F. M. F. de Groot, J. C. Fuggle, A. Fujimori, O. Strebel, F. Lopez, M. Domke, G. Kaindl, G. A. Sawatzky, M. Takano, Y. Takeda, H. Eisaki, and S. Uchida, "Controlled-valence properties of $La_{1-x}Sr_xFeO_3$ and $La_{1-x}Sr_xMnO_3$ studied by soft-x-ray absorption spectroscopy," *Phys. Rev. B*, vol. 46, pp. 4511–4519, 1992.

[23] F. M. F. de Groot, M. Grioni, J. C. Fuggle, J. Ghijsen, G. A. Sawatzky, and H. Petersen, "Oxygen 1 s XAS of transition metal oxides," *Phys. Rev. B.*, vol. 40, pp. 5715–5723, 1989.

[24] F. M. F. de Groot, J. C. Fuggle, B. T. Thole, and G. A. Sawatzky, "2p x-ray absorption of 3d transition metal compounds," *Phys. Rev. B*, vol. 42, pp. 5459–5468, 1989.

[25] M. Rini, Y. Zhu, S. Wall, R. I. Tobey, H. Ehrke, T. Garl, J. W. Freeland, Y. Tomioka, Y. Tokura, A. Cavalleri, and R. W. Schoenlein, "Transient electronic structure of the photoinduced phase of $Pr_{0.7}Ca_{0.3}MnO_3$ probed with soft x-ray pulses," *Phys. Rev. B*, vol. 80, p. 155113, 2009.

[26] S. S. Dhesi, A. Mirone, C. De Nadaï, P. Ohresser, P. Bencok, N. B. Brookes, P. Reutler, A. Revcolevschi, A. Tagliaferri, O. Toulemonde, and G. Van Der Laan, "Unraveling orbital ordering in $La_{0.5}Sr_{1.5}MnO_4$," *Phys. Rev. Lett.*, vol. 92, p. 056403, 2004.

[27] S. B. Wilkins, T. A. W. Beale, P. D. Hatton, J. A. Purton, P. Bencok, D. Prabhakaran, and A. T. Boothroyd, "Probing orbital order with soft x-rays: the case of the manganites," *New J. Phys.*, vol. 7, p. 80, 2005.

[28] C. W. M. Castleton and M. Altarelli, "Orbital ordering in the manganites: Resonant x-ray scattering predictions at the manganese LII and LIII edges," *Phys. Rev. B*, vol. 62, pp. 1033–1038, 2000.

[29] M. Matsubara, Y. Okimoto, T. Ogasawara, Y. Tomioka, H. Okamoto, and Y. Tokura, "Ultrafast photoinduced insulator-ferromagnet tran sition in the perovskite manganite $Gd_{0.55}Sr_{0.45}MnO_3$," *Phys. Rev. Lett.*, vol. 99, p. 207401, 2007.

[30] E. Dagotto, *Nanoscale, Phase Separation and Colossal Magnetoresistance*. Berlin: Springer, 2003.

[31] S. Wall, D. Prabhakaran, A. T. Boothroyd, and A. Cavalleri, "Ultrafast coupling between light, coherent lattice vibrations, and the magnetic structure of semicovalent $LaMnO_3$," *Phys. Rev. Lett.*, vol. 103, p. 097402, 2009.

[32] J. B. Goodenough, "Theory of the role of covalence in the perovskite-type manganites [La, M(II)]$MnO_3$," *Phys. Rev.*, vol. 100, pp. 564–573, 1955.

[33] N. N. Kovaleva, A. V. Boris, C. Bernhard, A. Kulakov, A. Pimenov, A. M. Balbashov, G. Khaliullin, and B. Keimer, "Spin-controlled mott-hubbard bands in $LaMnO_3$ probed by optical ellipsometry," *Phys. Rev. Lett.*, vol. 93, p. 147204, 2004.

[34] Y. Tokura, *Colossal Magnetoresistive Oxides*. Amsterdam: Gordon & Breach Science Publishers, 2000.

[35] M. Imada, A. Fujimori, and Y. Tokura, "Metal-insulator transitions," *Rev. Mod. Phys.*, vol. 70, pp. 70–1263, 1998.

[36] H. Y. Hwang, S-W. Cheong, P. G. Radaelli, M. Marezio, and B. Batlogg, "Lattice effects on the magnetoresistance in doped $LaMnO_3$," *Phys. Rev. Lett.*, vol. 75, pp. 914–917, 1995.

[37] M. Rini, Z. Hao Z, R. W. Schoenlein, C. Giannetti, F. Parmigiani, S. Fourmaux, J. C. Kieffer, A. Fujimori, M. Onoda, S. Wall, and A. Cavalleri, "Optical switching in $VO_2$ films by below-gap excitation," *Appl. Phys. Lett.*, vol. 92, p. 181904, 2008.

[38] A. V. Boris, N. N. Kovaleva, A. V. Bazhenov, A. V. Samoilov, N.-C. Yeh, and R. P. Vasquez, "Infrared optical properties of $La_{0.7}Ca_{0.3}MnO_3$ epitaxial films," *J. Appl. Phys.*, vol. 81, p. 5756, 1997.

[39] M. Rini, R. Tobey, N. Dean, J. Itatani, Y. Tomioka, Y. Tokura, R. W. Schoenlein, and A. Cavalleri, "Control of the electronic phase of a manganite by mode-selective vibrational excitation," *Nature*, vol. 449, pp. 72–74, 2007.

[40] M. Fiebig, K. Miyano, Y. Tomioka, and Y. Tokura, "Reflection spectroscopy on the photoinduced local metallic phase of $Pr_{0.7}Ca_{0.3}MnO_3$," *Appl. Phys. Lett.*, vol. 74, p. 2310, 1999.

[41] R. I. Tobey, R. Prabakharan, A. T. J. Boothroyd, and A. Cavalleri, "Ultrafast electronic phase transition in $La_{1/2}Sr_{3/2}MnO_4$ by coherent vibrational excitation: Evidence for nonthermal melting of orbital order," *Phys. Rev. Lett.*, vol. 101, p. 197404, 2008.

[42] R. W. Schoenlein, S. Chattopadhyay, H. H. W. Chong, T. E. Glover, P. A. Heimann, C. V. Shank, A. A. Zholents, and M. S. Zolotorev, "Generation of femtosecond pulses of synchrotron radiation," *Science*, vol. 287, pp. 2237–2240, 2000.

[43] A. L. Cavalieri, N. Müller, Th. Uphues, V. S. Yakovlev, A. Baltuska, B. Horvath, B. Schmidt, L. Blümel, R. Holzwarth, S. Hendel, M. Drescher, U. Kleineberg, P. M. Echenique, R. Kienberger, F. Krausz, and U. Heinzmann, "Attosecond spectroscopy in condensed matter," *Nature*, vol. 449, pp. 1029–1032, 2007.

[44] C. Kubler, H. Ehrke, R. Huber, R. Lopez, A. Halabica, R. F. Haglund, Jr., and A. Leitenstorfer, "Coherent structural dynamics and electronic correlations during an ultrafast insulator-to-metal phase transition in $VO_2$," *Phys. Rev. Lett.*, vol. 99, p. 116401, 2007.

[45] D. J. Hilton, R. P. Prasankumar, S. Fourmaux, A. Cavalleri, D. Brassard, M. A. El Khakani, J. C. Kieffer, A. J. Taylor, and R. D. Averitt, "Enhanced photosusceptibility near $T_c$ for the light-induced insulator-to-metal phase transition in vanadium dioxide," *Phys. Rev. Lett.*, vol. 99, p. 226401, 2007.

[46] L. Perfetti, P. A. Loukakos, M. Lisowski, U. Bovensiepen, H. Berger, S. Biermann, P. S. Cornaglia, A. Georges, and M. Wolf, "Time evolution of the electronic structure of 1 T-$TaS_2$ through the insulator-metal transition," *Phys. Rev. Lett.*, vol. 97, p. 067402, 2006.

[47] F. Schmitt *et al.*, "Transient electronic structure and melting of a charge density wave in $TbTe_3$," *Science*, vol. 321, p. 1649, 2008.

[48] A. Cavalleri, S. Wall, C. Simpson, E. Statz, D. W. Ward, K. A. Nelson, M. Rini, and R. W. Schoenlein, "Tracking the motion of charges in a terahertz light field by femtosecond X-ray diffraction," *Nature*, vol. 442, pp. 664–666, 2006.

[49] G. Sciaini, M. Harb, S. G. Kruglik, T. Payer, C. T. Hebeisen, F.-J. Meyer, zu Heringdorf, M. Yamaguchi, M. Horn-von Hoegen, R. Ernstorfer, and R. J. Dwayne Miller, "Electronic acceleration of atomic motions and disordering in bismuth," *Nature*, vol. 458, pp. 56–59, 2009.

**Simon Wall** was born in the U.K., in 1983. He received the Undergraduate M.Phys. degree in physics and the D.Phil. degree in "Photo-induced dynamics in complex materials probed with femtosecond X-rays and few-cycle optical pulses" from the University of Oxford, Oxford, U.K., in 2005 and 2009, respectively.

Since 2009, he has been with the Fritz Haber Institute, Berlin, Germany.

Dr. Wall became a Fellow of the Alexander von Humboldt Society in 2010.

**Matteo Rini** received the Ph.D. degree in electrical engineering from the University of Pavia, Pavia, Italy, in 2002, and the Ph.D. degree in physics from the Humboldt University and the Max Born Institute, Berlin, Germany, in 2003.

From 2004 to 2009, he worked at the Lawrence Berkeley National Laboratory, Berkeley, CA, where he was engaged in the application of ultrafast time-resolved techniques to complex solids. In 2009, he joined the Joint Research Centre, European Commission, Karlsruhe, Germany, as a Staff Scientist, where he is involved in the science and technology of actinide compounds.

**Sarnjeet S. Dhesi** received the Ph.D. degree in physics from the University of Liverpool, Liverpool, U.K., in 1993.

He was a Postdoctoral Fellow at the University of Liverpool and Boston University, Boston, MA from 1993 to 1997, a Staff Scientist at Daresbury Laboratory, Cheshire, England, U.K. from 1997 to 1999, and a Staff Scientist at the European Synchrotron Radiation Facility, Grenoble, France from 1999 to 2003. Since 2003, he has been a Principal Beamline Scientist at Diamond Light Source, Harwell Science and Innovation Campus, Chilton, Didcot, U.K. In 2006, he was a Visiting Professor in the Department of Physics and Astronomy, University of Leicester, Leicester, England. His research interests include the study of low-dimensional magnetism, magnetic anisotropy, and highly correlated systems using polarised X-rays.

**Robert W. Schoenlein** received the S.B., S.M., and Ph.D. degrees from the Massachusetts Institute of Technology, Cambridge, MA, in 1984, 1986, and 1989, respectively.

In 1989, he joined the Lawrence Berkeley National Laboratory, Berkeley, CA, where he is currently a Senior Staff Scientist and the Deputy Director for science at the Advanced Light Source, and has been engaged in active research programs in both the Materials Sciences and Chemical Sciences Divisions. His research interests include ultrafast X-ray spectroscopy and diffraction techniques to investigate atomic and electronic structural dynamics in condensed matter including transition-metal complexes, molecular dynamics in solution, and photoinduced phase transitions in correlated electron systems.

Dr. Schoenlein was the recipient of the Adolph Lomb Medal from the Optical Society of America in 1994.

**Andrea Cavalleri** received the Ph.D. degree in electrical engineering from the University of Pavia, Pavia, Italy, in 1998.

After Postdoctoral work at the University of California, San Diego from 1998 to 2001, he was a Physicist at the Lawrence Berkeley National Laboratory, Berkeley, CA from 2001 to 2005, a University Lecturer in physics from 2005 to 2006 and a Professor in physics from 2006 to 2008 at the University of Oxford, Oxford, U.K. Since 2008, he has been a Professor at the University of Hamburg, a Director at the Max Planck Department for Structural Dynamics—Centre for Free Electron Laser Science, Hamburg, Germany. His research interests include the studies of ultrafast physics and quantum phase control in complex solids, combining femtosecond techniques that span the entire electromagnetic spectrum, from terahertz to the hard X-rays.

## DISCLAIMER